

# Ultraviolet and optical view of galaxies in the Coma Supercluster

Smriti Mahajan<sup>\*</sup>, Ankit Singh, Devika Shobhana

*Indian Institute for Science Education and Research Mohali - IISERM, Knowledge City, Manauli, 140306, Punjab, India*

Accepted XXX. Received YYY; in original form ZZZ

## ABSTRACT

The Coma supercluster ( $100h^{-1}\text{Mpc}$ ) offers an unprecedented contiguous range of environments in the nearby Universe. In this paper we present a catalogue of spectroscopically confirmed galaxies in the Coma supercluster detected in the ultraviolet (UV) wavebands. We use the arsenal of UV and optical data for galaxies in the Coma supercluster covering  $\sim 500$  square degrees on the sky to study their photometric and spectroscopic properties as a function of environment at various scales. We identify the different components of the cosmic-web: large-scale filaments and voids using Discrete Persistent Structures Extractor, and groups and clusters using Hierarchical Density-based spatial clustering of applications with noise, respectively. We find that in the Coma supercluster the median emission in  $\text{H}\alpha$  inclines, while the  $g-r$  and  $FUV-NUV$  colours of galaxies become bluer moving further away from the spine of the filaments out to a radius of  $\sim 1$  Mpc. On the other hand, an opposite trend is observed as the distance between the galaxy and centre of the nearest cluster or group decreases. Our analysis supports the hypothesis that properties of galaxies are not just defined by its stellar mass and large-scale density, but also by the environmental processes resulting due to the intrafilament medium whose role in accelerating galaxy transformations needs to be investigated thoroughly using multi-wavelength data.

**Key words:** catalogues; galaxies: clusters: general; galaxies: evolution; galaxies: fundamental parameters; galaxies: star formation; ultraviolet: galaxies

## 1 INTRODUCTION

Large-scale cosmic-web filaments are crucial, yet poorly investigated intermediate density environments capable of accelerating galaxy transformation (Porter et al. 2008; Haines et al. 2011; Alpaslan et al. 2016; Martínez, Muriel, & Coenda 2016; Kuutma, Tamm, & Tempel 2017). Studies at high redshift (Fadda et al. 2008; Geach et al. 2011; Coppin et al. 2012; Darvish et al. 2014) as well as  $z \sim 0$  (e.g. Porter et al. 2008; Mahajan, Haines, & Raychaudhury 2010; Haines et al. 2011; Alpaslan et al. 2016; Kim et al. 2016; Kleiner et al. 2017; Kuutma, Tamm, & Tempel 2017; Kraljic et al. 2018) have now shown that the intermediate density environment prevalent in filaments not just bridge the gap between the dense interior of clusters and ‘voids’ devoid of galaxies, but play a rather important role in modulating galaxy observables. Owing to the highly coherent flow of galaxies along the filaments (González & Padilla 2009), they have not just been observed at all wavelengths

from ultraviolet (UV) (Gallazzi et al. 2009; Geach et al. 2011; Coppin et al. 2012) to infrared (Fadda et al. 2008; Haines, Gargiulo, & Merluzzi 2008) by direct methods such as quantifying the distribution of galaxies, thermal Sunyaev-Ze’ldovich (tSZ) effect (Bonjean et al. 2018) and weak gravitational lensing (Dietrich et al. 2012; Jauzac et al. 2012), but also indirectly using a bent double lobe radio source (Edwards, Fadda, & Frayer 2010b).

Recently, filaments, in particular the warm hot intergalactic medium (WHIM) in filaments has been the pivot of several studies. Using emission in the soft x-ray bands, such studies estimate the WHIM temperature in filaments to be  $\sim 3-8$  keV (Eckert et al. 2015; Akamatsu et al. 2017; Parekh et al. 2017; Tanimura et al. 2017). Furthermore, the cosmic microwave background map from the Planck together with the Canada France Hawaii Telescope Lensing Survey, as well as the Two-Micron All-Sky Redshift Survey of galaxies suggest that at least half of the missing baryons in the Universe may reside as WHIM in large-scale filaments tracing the dark matter distribution (Van Waerbeke, Hinshaw, & Murray 2014; Génova-Santos et al. 2015). Therefore, undeniably it is cru-

<sup>\*</sup> E-mail: smritimahajan@iisermohali.ac.in

cial to characterise the large-scale structure (LSS) of the Universe and comprehend the impact of the cosmic-web on properties of galaxies.

The Coma supercluster is one of the richest large-scale structure (Chincarini & Rood 1976) in the nearby Universe comprising two clusters of galaxies, connected by a web of large-scale filaments around  $30h_{70}^{-1}$  Mpc long (e.g. Fontanelli 1984). The two clusters, Coma (Abell 1656) and Abell 1367, along with the filaments of galaxies, dispersed with several small galaxy groups span  $\sim 500$  square degrees on the sky (Mahajan, Haines, & Raychaudhury 2010). The large-scale filaments in the Coma supercluster have not just been observed by means of the galaxy distribution in the optical wavebands (Gregory & Thompson 1978; Mahajan, Haines, & Raychaudhury 2010), but also diffuse emission in the radio continuum (Kim et al. 1989).

Studies of clusters and groups at  $z \sim 0$  have evidently shown that outskirts of groups and clusters (Zabludoff & Mulchaey 1998; Rines et al. 2005; Wang, Owen, & Ledlow 2004; Cortese et al. 2007; Tran et al. 2009; Gavazzi et al. 2010; Smith et al. 2010; Sun et al. 2010; Coppin et al. 2011; Mahajan, Raychaudhury, & Pimblet 2012; Verdugo et al. 2012; Mahajan 2013) and filaments of galaxies (Porter & Raychaudhury 2007; Boué et al. 2008; Fadda et al. 2008; Porter et al. 2008; Edwards et al. 2010a; Biviano et al. 2011) are favourable sites for galaxy transformations. Based on a study using optical data from the Sloan Digital Sky Survey (SDSS) data release (DR) 7, Mahajan, Haines, & Raychaudhury (2010) found that the star formation-density relation in the Coma supercluster for the giant galaxies is much weaker than their dwarf counterparts. However, the fraction of star-forming galaxies for both declines to  $\sim 0$  at the centre of the clusters (also see Mahajan, Haines, & Raychaudhury 2011). Cybulski et al. (2014) furthered the study of star formation in the Coma supercluster by combining a complementary optical dataset from SDSS DR 9, with IR data from the *Wide-Field Infrared Survey Explorer* (WISE; Wright et al. 2010) and UV data from the *Galaxy Evolution Explorer* (GALEX; Martin et al. 2005). Cybulski et al. (2014) corroborated the results of Mahajan, Haines, & Raychaudhury (2010, 2011) by probing both obscured and unobscured star formation down to  $\sim 0.02 M_{\odot} \text{ yr}^{-1}$ , in order to quantify the effect of different types of large-scale environments: groups, clusters, filaments and voids, on quenching star formation (SF) in galaxies.

In the absence of dust in star-forming galaxies, the UV emission is a good tracer of massive ( $> 10M_{\odot}$ ) star formation. On the other hand, optical emission lines such as H $\alpha$  probe instantaneous star formation over a time-scale of  $\lesssim 20$  Myr (Kennicutt 1998). Assuming that the UV luminosity is not overwhelmed by contribution from the old stellar populations due to the UV upturn such as in massive early-type galaxies (O’Connell 1999), the UV luminosity measures star formation over a timescale of  $\sim 100$  Myr (Kennicutt 1998). Hence, the star formation rate (SFR) estimated from optical emission lines delineates the continuous SF in a galaxy, while the SFR determined from the UV is representative of its recent SF activity. But even though GALEX and its predecessor UV imagers have been used to investigate individual galaxies within clusters and groups (e.g. Hicks & Mushotzky

2005), or galaxy populations therein (e.g. Donas et al. 1990; Donas, Milliard, & Laget 1995; Cornett et al. 1998; Boselli et al. 2005b), limited work has been done to analyse the UV properties of galaxies in the large-scale cosmic-web.

Since the Coma supercluster is one of the most well studied regions in the nearby Universe, many other authors (e.g. Bernstein et al. 1995; Mobasher et al. 2003; Hammer et al. 2012; Smith et al. 2010; Smith, Lucey, & Carter 2012) have made use of optical and UV data to study the Coma and Abell 1367 clusters and their surroundings. With the advent of large redshift surveys several studies (Gavazzi et al. 2010; Mahajan, Haines, & Raychaudhury 2010, 2011; Cybulski et al. 2014; Gavazzi et al. 2013) have also used multi-wavelength data at optical, UV and 21 cm continuum to study the properties of galaxies in the entire supercluster region. In this paper we make use of similar datasets: UV data derived from GALEX and optical spectroscopic and photometric data from the SDSS for the entire Coma supercluster to further explore the impact of environment on the properties of galaxies.

Conventionally, the ‘environment’ of galaxies is quantified as the projected density of galaxies in a fixed 2-d or 3-d region of the sky (e.g. Dressler 1980). Muldrew et al. (2012) combined 20 published methods of defining environment into two (i) methods which use nearest-neighbours to probe the underlying galaxy density and, (ii) fixed aperture methods. Muldrew et al. (2012) found that while the former are better suited for quantifying internal density within massive halos, the latter, fixed-aperture methods are better for probing the large-scale environment. Therefore, in order to characterise the large-scale cosmic-web, a combination of these methodologies is required to quantify the environment on different scales. In this work we implement their result by making use of two different algorithms to define the large-scale filaments, and high density nodes of the cosmic-web characterised as clusters and groups. We also present a catalogue of all spectroscopically-confirmed galaxy members of the Coma supercluster detected in the UV.

This paper is organised as follows: in the next section we describe our datasets, followed by definition of environment in Sec. 3. In Sec. 4 we analyse the broadband colours of galaxies as a function of environment, while in Sec. 5 we study the impact of the large-scale filaments on the properties of galaxies. Finally, we discuss our results in the context of the existing literature in Sec. 6 and summarise our results in Sec. 7. Throughout this paper we use concordance  $\Lambda$ CDM cosmological model with  $H_0 = 70 \text{ km s}^{-1} \text{ Mpc}^{-1}$ ,  $\Omega_{\Lambda} = 0.7$  and  $\Omega_m = 0.3$  to calculate distances and magnitudes. We note that at the redshift of the Coma cluster ( $z = 0.023$ ) our results are independent of the cosmological model used.

## 2 DATA

This work is based on the optical photometric and spectroscopic data acquired from the SDSS data release 12 (Alam et al. 2015), and UV data from the GALEX survey (Bianchi, Conti, & Shiao 2014). In the following we describe both the datasets used in this work.

## 2.1 Optical data

The Sloan Digital Sky Survey (SDSS) uses two fibre-fed double spectrographs, covering a wavelength range of 3800–9000 Å. The resolution  $\lambda/\Delta\lambda$  varies between 1500 and 2500 in different bands. Galaxy magnitudes<sup>1</sup> are *K*-corrected to  $z = 0$  (Chilingarian & Zolotukhin 2012), and for galactic extinction. For the latter, the  $E(B - V)$  values in each of the *g* and *r* bands are calculated using the Schlegel (1998) dust maps.

Following Mahajan, Haines, & Raychaudhury (2010), we select all galaxies brighter than  $m_r = 17.77$  mag and spectroscopic data which lie within  $170^\circ \leq \text{RA} \leq 200^\circ$ ,  $17^\circ \leq \text{Dec} \leq 33^\circ$  and  $0.013 \leq z \leq 0.033$ . These criteria yield a total of 4,280 galaxies. In this work we use the equivalent width of the H $\alpha$  emission line as an indicator of the instantaneous (< 10 Myr) star formation rate (SFR) of galaxies.

The spectra of 86% of all the galaxies in the Coma supercluster have all four emission lines (H $\alpha$ , [NII], H $\beta$  and [OIII]) required to confirm the presence of nuclear activity based on the emission-line ratio diagnostics as first proposed by Baldwin, Phillips, & Terlevich (1981). For this work, we use the classification criteria of Kewley et al. (2001) to identify 518 (~ 12%) galaxies as AGN. Where applicable, we perform the analysis using non-AGN galaxies only i.e. the entire sample minus the 518 galaxies whose spectra is dominated by AGN emission.

## 2.2 Ultraviolet data

The ultraviolet photometric data for this work is taken from the *Galaxy Evolution EXplorer* final data release (*GALEX*; Bianchi, Conti, & Shiao 2014). *GALEX* conducted an all-sky imaging survey along with targeted programs in two photometric bands: 1516 Å (“far ultraviolet” or *FUV*) and 2267 Å (“near ultraviolet” or *NUV*). The bulk of our sample consists of bright, nearby galaxies, and therefore no exposure time or brightness limit constraints were imposed while looking for a *GALEX* detection. For best photometric and astrometric quality we have restricted our sample to the inner 0.5° of the *GALEX* field of view and having  $\text{NUV\_artifact} < 1$ . As suggested by Wyder et al. (2007), the latter excludes objects whose flux may be contaminated by reflection from bright stars.

65% of the UV imaging data used in this paper were taken as part of the *GALEX*’s primary All-Sky Imaging Survey (AIS) with an effective exposure time of ~0.1 ks. Most of the rest of the data comes from individual guest investigator programs (28%) or the Nearby Galaxies Survey (NGS; 6%) with an effective exposure time of ~1.5 ks. The remaining data was taken as part of *GALEX*’s medium or deep imaging surveys (MIS and DIS), having an average exposure time of ~1.5 and 30 ks respectively.

We searched for the UV counterpart of each spectroscopically-confirmed supercluster galaxy within a circular aperture with radius 4'' centred on the optical source

(Budavári et al. 2009). Amongst others, this process also yields 477 optical sources multiply matched to many UV sources. Following Bianchi et al. (2011), we considered the multiply-matched UV sources as duplicates if they were within 2.5'' of each other. Of those UV sources which satisfied this criteria, if the *photoextractid* of both the UV sources is the same implying both of them are from the same observation, they were both considered unique, else they were assumed to be multiple observations of the same source. In the former case, the matched counterpart was represented by the UV source with the highest *NUV* exposure time. In case of equal *NUV* exposure times for both, the one closest to the field centre in the *GALEX* image was chosen.

For the *FUV* and *NUV* photometry we used Kron magnitudes generated by the *GALEX* pipeline and corrected for galactic extinction using Schlegel (1998) dust maps, assuming the reddening law of Cardelli, Clayton, & Mathis (1989). The reddening factor for *GALEX* bands is  $AFUV/E(B - V) = 8.24$  mag and  $ANUV/E(B - V) = 8.2$  mag (Wyder et al. 2007), respectively, which lead to a median extinction correction of ~ 0.23 mag in both the UV bands. Since *GALEX* colour is an important part of our analysis, we chose the *NUV* band as the primary band and then obtained the corresponding *FUV* magnitude measured within the same Kron aperture as estimated using the *NUV* image to get an accurate UV colour.

Hammer et al. (2010) have created a source catalogue of objects detected in a 26 ks deep *GALEX* field in the Coma cluster. For 94 galaxies (matched within 10'') of their sources, we find a median offset of 0.1 mag in the *FUV* and 0.2 mag in the *NUV* magnitudes, respectively. The discrepancy in the measured magnitudes is due to the bayesian deblending technique used by these authors, since the photometry thus obtained is relatively more sensitive to the apparent sizes of galaxies, and underestimates the flux for extended ( $R_{90,r} > 10''$ ) galaxies (Hammer et al. 2010), which make up > 50% of our sample.

Our final UV catalogue comprises 2,447 UV sources uniquely matched to spectroscopically-confirmed SDSS galaxies in the Coma supercluster region. The combined optical-UV data are shown in Figure 1, and the data for all 4,280 galaxies are given in Table 1. The columns in Table 1 are: (i) Plate, (ii) MJD, (iii) Fibre ID, (iv) *GALEX* ID, (v) Right ascension (J2000), (vi) Declination (J2000), (vii) redshift (viii) local environment (0: void, 1: filaments and 2: cluster/group), (ix) *r*-band magnitude (x) *FUV* magnitude, (xi) error in *FUV* magnitude, (xii) *NUV* magnitude and (xiii) error in *NUV* magnitude. The first three columns can be used to crossmatch galaxy data with the SDSS database, while the unique *GALEX* ID can be used for the same with the *GALEX* database.

Since we are covering such a large chunk of the sky (~ 500 sq. degrees), it is unsurprising that the depth of *GALEX* observations varies widely over the entire supercluster. Cybulski et al. (2014, see their sec. 2.2 for details), have shown that the *GALEX* data for the Coma supercluster is 75% complete to a luminosity of ~ 26.42 ergs. We therefore stress that our UV catalogue is incomplete for two major reasons: firstly, due to incomplete spatial coverage of *GALEX* due to the presence of bright foreground sources (e.g. region around  $\alpha \sim 186^\circ$  and  $\delta \sim 26^\circ$  in Figure 1). Secondly, as shown in Figure 2 only ~ 60% of the

<sup>1</sup> Throughout this paper we use the SDSS ‘model’ magnitudes. The model magnitude for each galaxy is calculated using the best-fit parameters in the *r* band, and applied to all other bands; the light is therefore measured consistently through the same aperture in all bands, allowing for an unbiased measure of galaxy’s colours.

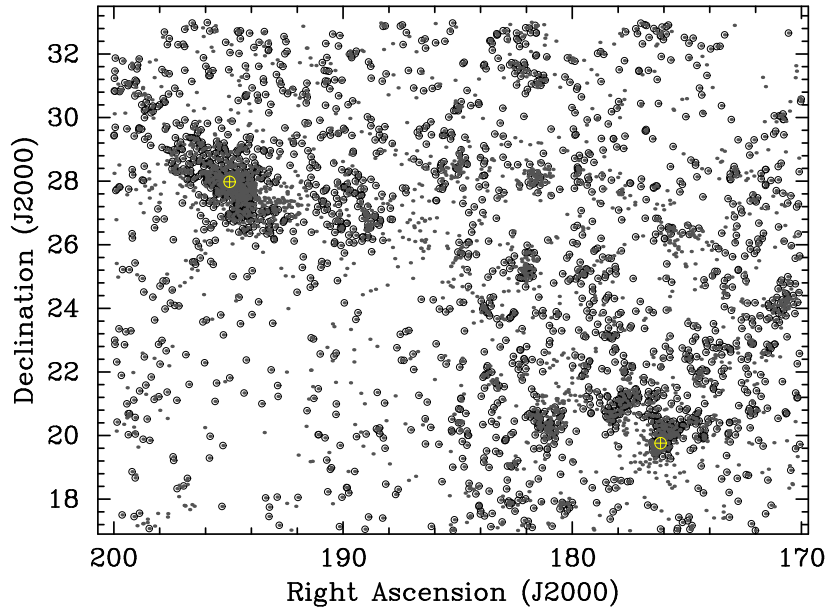


**Figure 1.** The Coma supercluster. All spectroscopically confirmed galaxies are represented as *dots*, and all galaxies with a UV counterparts are *encircled*. The *yellow encircled crosses* represent the centre of the Coma and Abell 1367 clusters.

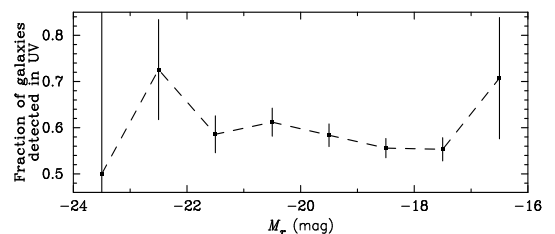
**Table 1.** The SDSS and *GALEX* data for all the Coma supercluster galaxies in our sample. The local environment of galaxies listed in column 8 is: 0: void, 1: filaments and 2: cluster/group, respectively. See section 3 for detailed definition of these environments.

Plate	MJD	Fiber	<i>GALEX</i> ObjID	RA (J2000)	Dec (J2000)	z	Local env	$M_r$ mag	$m_{NUV}$ mag	$\Delta m_{NUV}$ mag	$m_{FUV}$ mag	$\Delta m_{FUV}$ mag
2241	54169	562	-	195.547	28.172	0.0299	2	-18.69	-	-	-	-
2241	54169	517	3191682282023817108	194.984	27.746	0.0298	2	-19.43	19.05	0.02	19.69	0.03
2240	53823	530	-	194.629	28.234	0.0243	2	-19.18	-	-	-	-
2240	53823	617	3187917554210322283	195.170	27.997	0.0236	2	-20.67	20.61	0.02	22.07	0.06
2509	54180	226	-	176.020	19.533	0.0243	2	-18.63	-	-	-	-
2506	54179	548	2555795125061031411	176.134	20.107	0.0240	2	-20.05	19.87	0.04	20.67	0.07
2242	54153	384	3054146571327246615	195.313	27.669	0.0236	2	-18.64	22.01	0.15	23.13	0.38
2241	54169	573	-	195.406	28.016	0.0238	2	-18.07	-	-	-	-
2241	54169	371	-	194.523	28.243	0.0240	2	-21.39	-	-	-	-
2240	53823	518	-	194.548	27.940	0.0284	2	-19.45	-	-	-	-

spectroscopically-confirmed galaxies are detected in each bin of  $r$ -band magnitude. However, since the fraction of galaxies missing a UV counterpart is almost uniform across the entire luminosity range, except the lowest and the highest luminosity bin comprising 2 and 41 galaxies respectively, we have not corrected for this incompleteness in the following analysis. We use all the UV-detected galaxies for all UV-based analysis, and all spectroscopically-confirmed galaxies for all the optical analysis below.

### 3 THE ENVIRONMENT

It is now well established that the Coma supercluster comprises of a filamentary network including the two major clusters Coma and Abell 1367, and other smaller galaxy groups (Gregory & Thompson 1978; Mahajan, Haines, & Raychaudhury 2010). This filamentary network has been mapped by the distribution of galaxies as well as observed in the radio continuum at 326 MHz (Kim et al. 1989). In the following sections we will analyse optical and ultraviolet properties of galaxies in the Coma



**Figure 2.** Fraction of Coma supercluster galaxies with a UV counterparts in bins of absolute  $r$ -band magnitude. On average,  $\sim 60\%$  of the galaxies are detected by *GALEX* in each bin of  $M_r$ . The error bars on each point represent Poissonian uncertainty.

supercluster as a function of their environment. In order to do so, we first modelled the complex cosmic-web of the Coma supercluster by identifying its various components as described below.

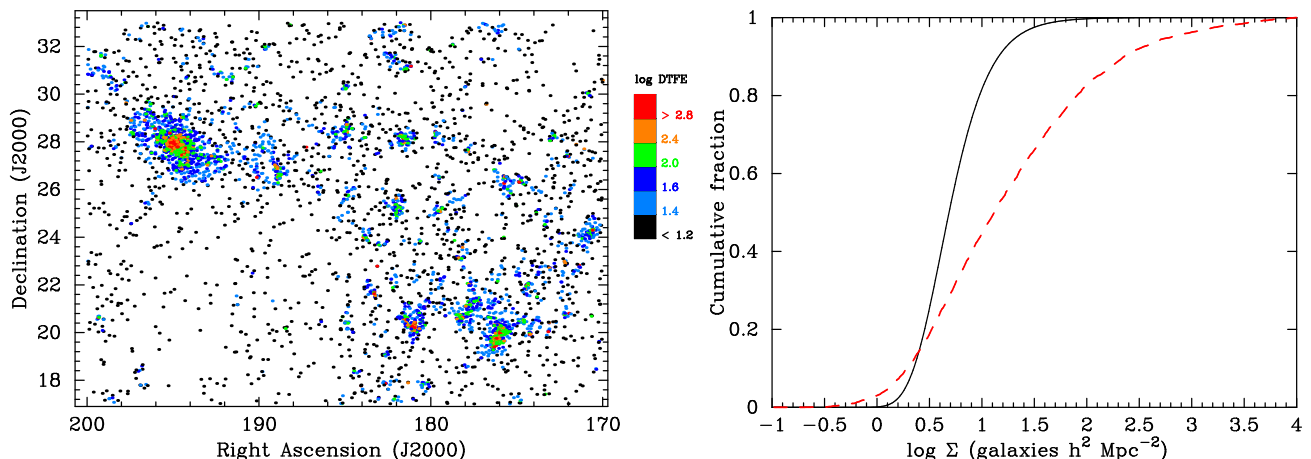


**Figure 3.** (*left:*) The Coma supercluster galaxies colour-coded with log of Delaunay Tessellation Field Estimator value (see text). (*right:*) The mean cumulative distribution of the DTFE density for the random samples (*black solid line*) compared with the same for the Coma supercluster (*red dashed line*). The Coma supercluster region is not just denser relative to the random distributions, but also comprise very over-dense (clusters and groups) and under-dense (voids) regions.

### 3.1 The cosmic-web with DISPERSE

The filaments in the Coma supercluster in this work are defined using Discrete Persistent Structures Extractor (DISPERSE; Sousbie 2011), which is an algorithm capable of finding structures, in particular linear structures such as large-scale filaments within discrete 2d or 3d datasets (see Sousbie, Pichon, & Kawahara 2011b, for illustrations of DISPERSE in the astrophysical context). DISPERSE allows us to work directly with particles, and requires only one tunable parameter corresponding to the significance of the retained features in units of  $\sigma^2$ . Furthermore, DISPERSE does not make any presumptions about the quality of sampling, homogeneity or topology of the space.

DISPERSE is based on discrete Morse theory and persistence homology theory. The Delaunay tessellation is used to segregate the whole space into triangular regions. The Delaunay Tessellation Field Estimator (DTFE; Schaap & van de Weygaert 2000; Cautun & van de Weygaert 2011) allows the estimation of density at each vertex of the triangular complexes created by Delaunay tessellation. The estimated density can then be used in the Morse theory to identify the critical points where the gradient of density field vanishes.

The topology of a function can be studied using the topology of points which are above a continuous monotonically changing threshold. If the persistence value of a pair of critical points is higher than the noise level defined by the root mean square of persistence values of randomly selected points, the detected feature tends to have a significant density contrast. One can select a threshold of persistence values above which the pairs are to be considered for analysis. This enables extraction of all significant features in the space while eliminating noise. The filaments can be identified as lines connecting two maximas residing at the centres of groups and cluster regions. For a detailed discussion of the

theoretical framework which forms the basis for DISPERSE, we refer the reader to Sousbie (2011).

In Figure 3 (left) we show the position of all galaxies colour-coded by their DTFE value. Following Cybulski et al. (2014), we generated 1500 random samples of galaxy densities with the same number of galaxies as in the Coma supercluster, but their positions distributed randomly. Figure 3 (right) shows a comparison between the cumulative distribution of the mean of the galaxy density of 1500 random samples with the Coma supercluster. This figure is directly comparable to figure 4 (right) of Cybulski et al. (2014). Since we have used a dataset very similar to theirs, we also observe trends similar to those seen by Cybulski et al. (2014). The densities in the Coma supercluster gradually increases from a few to  $\sim 100 - 1000$  galaxies per square Mpc.

Figure 3 shows that the Coma supercluster on average is denser than a randomly selected region of the Universe, in the sense that the median density of galaxies in the supercluster is  $\sim 0.4$  dex higher relative to the mean of random samples. These observations are well in agreement with other studies (Gavazzi et al. 2010), reporting that with a mean density of  $0.019 \text{ gal } (h^{-1} \text{ Mpc})^{-3}$  the Coma supercluster is three times over-dense relative to the Universe in general ( $0.006 \text{ gal } h^{-3} \text{ Mpc}^{-3}$  for  $M_i < -19.5 \text{ mag}$ ; Hogg et al. 2004).

### 3.2 Identifying Galaxy Groups

Along with the clusters and the cosmic-web, another prominent environment in the Coma supercluster is of galaxy groups. In this work we identify the galaxy groups by Hierarchical Density-Based Spatial Clustering of Applications with Noise (HDBSCAN<sup>3</sup>; McInnes, Healy & Astels 2017b). HDBSCAN is a theoretically and practically improved version of the popular Density-based spatial clustering of applications with noise (DBSCAN) algorithm (Ester et al. 1996; Schubert et al. 2017).

<sup>2</sup> In this work we use a significance threshold of  $3\sigma$  which corresponds to a probability of  $\sim 0.997$  (Sousbie 2011).

<sup>3</sup> Specifically we adopted the Python implementation of HDBSCAN

DBSCAN requires minimal domain knowledge to determine input parameters, and works efficiently on large datasets. For our work, DBSCAN is a better choice relative to other unsupervised clustering algorithms (e.g. k-means) because of its ability to detect arbitrarily shaped clusters. The functioning of the algorithm is primarily governed by two parameters, `minPts` (minimum number of data points to be considered as a ‘cluster’) and  $\epsilon$  (the maximum radius permissible for a cluster). To begin with, DBSCAN classifies the data into three categories: core points (points with the maximum number of `minPts` in their vicinity), border points (points with lesser number of `minPts` but in the vicinity of a core point), and outliers (all other data points). The main issue with this approach is that the points which are in the vicinity of more than one core points, will have equal probability of being assigned to either of the clusters. Another drawback of the DBSCAN algorithm is that it is inefficient in finding clusters in an inhomogeneous dataset, making it very difficult to select the initial parameters for the algorithm.

HDBSCAN improves upon the methodology of the DBSCAN algorithm by extracting flat clustering based on stability of clusters (Campello et al. 2013). The main governing clustering parameter in HDBSCAN is `min_cluster_size` (the minimum size of an allowed cluster), which is chosen by the user based on the knowledge of the dataset. Another parameter which is crucial in deciding the final clustering is `min_samples`, which sets how conservative the clustering should be. By default `min_samples` is set equal to `min_cluster_size`, but can be tuned to suit the dataset. A very large value of `min_samples` will label most of the data points as noise, where as setting it as unity will allow all the data points to be clustered. In this work we adopt `min_sample_size` = 20 and `min_samples` = 10. The working of HDBSCAN can intuitively be divided into five steps:

- calculation of the *mutual reachability distance* (Campello et al. 2015) for all the data points, where, the mutual reachability distance between two points  $a$  and  $b$  is defined as the maximum of the distance to the  $k$ th nearest neighbour for  $a$ ,  $b$  or the distance between  $a$  and  $b$ , i.e.  $d_{mutual}(a, b) = \max\{\text{core}_k(a), \text{core}_k(b), d(a, b)\}$ ,
- construction of the minimum spanning tree of the data points weighted by their mutual reachability distance,
- building the hierarchy of the connected components,
- depending on the minimum size of the cluster allowed (`min_cluster_size`), HDBSCAN condenses and retains the clusters having size greater than `min_cluster_size`. This step significantly reduces the number of branches relative to the previous step; and
- the clusters which persist longer than their descendant clusters in the hierarchy tree are chosen as stable clusters and their descendants are disregarded, else the descendant clusters are chosen as stable clusters.

The final step allows HDBSCAN to select clusters with varying density.

### 3.3 Characterisation of environment

For further analysis of galaxy properties as a function of their environment, we segregate the Coma supercluster into three ‘local’ environments:

- Cluster/group galaxies (2,401): all galaxies identified by HDBSCAN to lie in groups or clusters. For simplicity, hereafter we refer to all the galaxies in these environments as cluster galaxies.
- Filament galaxies (766): all galaxies which are within a radius of 1 Mpc of the filamentary spine (see Sec. 5 for details on the choice of filament radius) detected by DISPERSE.
- Void galaxies (1,113): all other galaxies which lie within  $170^\circ \leq \text{RA} \leq 200^\circ$ ,  $17^\circ \leq \text{Dec} \leq 33^\circ$ , and have redshift  $0.013 \leq z \leq 0.033$ , but are not selected in either of the above two categories.

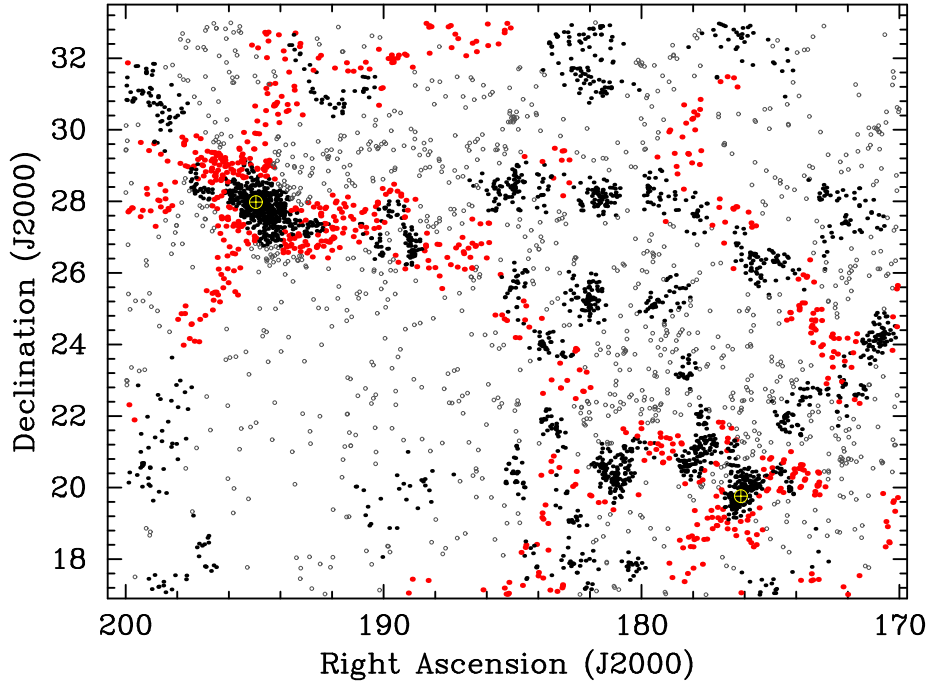
Figure 4 shows the projected distribution of galaxies belonging to various environments in the Coma supercluster.

## 4 BROADBAND COLOURS OF GALAXIES IN DIFFERENT ENVIRONMENTS

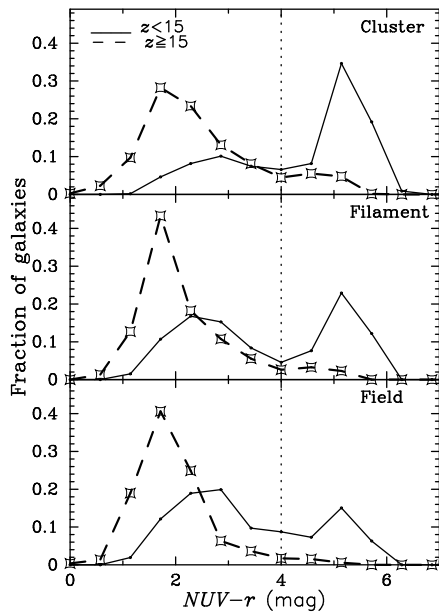
In this section we test the impact of local environment (Sec. 3) on optical and UV colours of galaxies. It is worth noting that although such studies have been conducted for various samples of groups and clusters at different redshifts, no other large-scale structure offers such a *continuous range of ‘local’ environments* in the nearby Universe (e.g. Gavazzi et al. 2010; Mahajan, Haines, & Raychaudhury 2010; Cybulski et al. 2014). The proximity of the Coma supercluster also makes it a special laboratory to investigate the properties of not just the giant, but also the dwarf galaxies. But since  $M^*$  is well correlated with environment (e.g. Haines et al. 2007), and may be the underlying property governing other galaxy observables (Kauffmann et al. 2003), where applicable we perform the following analysis in three classes of environments and two bins of luminosity. For the latter we divide our sample into dwarfs ( $z \geq 15$  mag) and giants ( $z < 15$ ) following Mahajan, Haines, & Raychaudhury (2010). At the redshift of the Coma cluster ( $z = 0.023$ ),  $z = 15$  mag corresponds to a  $M^* \sim 10^{9.5} M_\odot$ .

Figure 5 shows the distribution of the  $NUV-r$  colour for the dwarf and giant galaxies in the three different environments in the Coma supercluster. As expected, the fraction of red giants declines, while that of the dwarfs increases as the density of environment reduces. The dwarfs are almost always blue except in the densely populated clusters and groups, although in much fewer numbers than their giant counterparts. Wyder et al. (2007, also see Schawinski et al. (2007)) found the  $NUV-r$  distribution of SDSS galaxies to be bimodal around  $NUV-r \sim 4$  mag. Using their criteria we find 38%, 20% and 13% of all UV-detected galaxies in clusters, filaments and voids are passive (i.e.  $NUV-r > 4$  mag) in our sample, respectively.

Fig. 6 shows the distribution of non-AGN galaxies in the  $NUV-r$  versus  $M_r$  colour-magnitude space for the three different environments. Here we divide the sample into passive and star-forming galaxies around  $H\alpha$  equivalent width (EW) = 2 Å (e.g. Haines, Gargiulo, & Merluzzi 2008). The colour-magnitude relation fitted to passive galaxies in clusters takes the form  $NUV-r = 0.94 - 0.22M_r$ , with a dispersion of 0.63 mag. This figure evidently shows the strengthening of the red sequence as the environment becomes denser. We note that in all environments galaxies with  $NUV-r \lesssim 4$  mag are almost always spectroscopically star-forming. It is also



**Figure 4.** Different environments in the Coma supercluster. The *grey open circles*, *red points*, and *black points* represent the void, cosmic-web and cluster galaxies, respectively. The *yellow encircled crosses* represent the centre of the Coma and Abell 1367 clusters.



**Figure 5.** The  $NUV - r$  colour distribution of dwarf ( $z \geq 15$ ) and giant ( $z < 15$ ) galaxies in three different environments in the Coma supercluster.

notable that despite a small population of passive galaxies in the filament region, the distinction between the red sequence and the blue cloud is much clearly visible in the filaments relative to the void sample.

These observations are in agreement with the results of Gavazzi et al. (2010), who made use of the  $M_i$  vs  $g-i$  colour-magnitude relation to show that the red sequence becomes more apparent and the fraction of blue galaxies declines with increasing environmental density. Similar trends have also

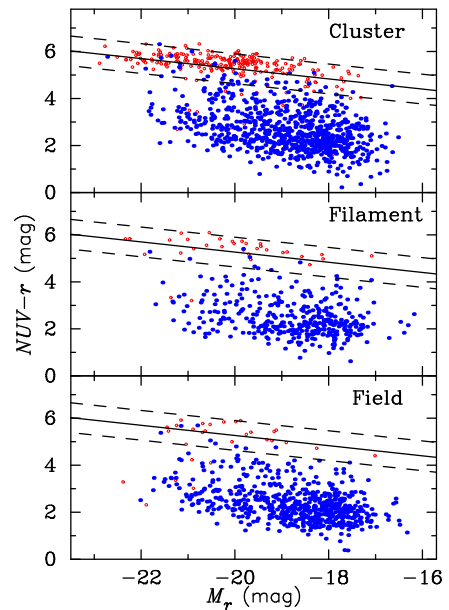


**Figure 6.** The  $NUV - r$  versus  $M_r$  colour-magnitude diagram for the galaxies in three different environments in the Coma supercluster. The points are colour-coded as: passive galaxies ( $EW(H\alpha) \leq 2 \text{ \AA}$ ) as *open red symbols*, and star-forming galaxies ( $EW(H\alpha) > 2 \text{ \AA}$ ) as *blue points*. The red sequence fitted to the passive galaxies in clusters are repeated in the other two panels.

been observed in and around the Virgo cluster, where using the  $NUV - i$  colour Boselli et al. (2014) showed that the red sequence is well established in the low density outskirts of the cluster, albeit with a much lower fraction of red galaxies relative to their star-forming counterparts.

Overall, in agreement with the literature (e.g.

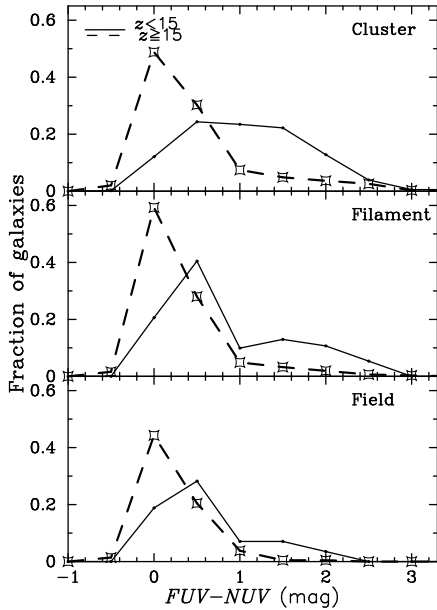


**Figure 7.** The  $FUV - NUV$  colour distribution of dwarf ( $z \geq 15$ ) and giant ( $z < 15$ ) galaxies in three different environments in the Coma supercluster.

Wyder et al. 2007; Haines, Gargiulo, & Merluzzi 2008) Fig. 6 shows that the position of a galaxy in the  $NUV - r$  versus  $M_r$  colour-magnitude space can be robustly used to distinguish the star-forming galaxies from their passively-evolving counterparts.

The trends seen for  $NUV - r$  also continue in the distribution of the  $FUV - NUV$  distributions in different environments as shown in Figure 7. The UV colour is a good proxy for young massive stars formed recently in star-forming galaxies. In the passively-evolving galaxies the  $FUV$  emission is dominated by evolved stellar populations, and hence correlates well with both age and metallicity of the dominating stellar population with surprisingly little scatter (Burstein et al. 1988; O’Connell 1999; Boselli et al. 2005b; Smith, Lucey, & Carter 2012). Therefore as expected, the fraction of massive galaxies having  $FUV - NUV \gtrsim 1$  mag increases from 27% in the field to 63% in the clusters with the filaments bridging the gap in between with the fraction of red galaxies = 39%. The dwarfs on the other hand are relatively bluer than their giant counterparts in all environments, with the fraction of galaxies with  $FUV - NUV \gtrsim 1$  mag being 19%, 11% and 7% in the clusters, filament and field region respectively. Segregating galaxies by their SF activity based on  $EW(H\alpha)$ , Cortese et al. (2005) also observed similar trends for the galaxies in Abell 1367 such that the star-forming galaxies dominate at high UV luminosities, while the quiescent ones contribute at the faint end of the UV luminosity function.

All galaxies detected in UV are shown in the  $NUV - r$  versus  $FUV - NUV$  colour-colour distribution in Fig. 8. While  $NUV - r$  and  $FUV - NUV$  become redder together for the blue galaxies ( $EW(H\alpha) \geq 2\text{\AA}$ ), the  $NUV - r$  is always between 5–6 mag for passively-evolving galaxies independent of their  $FUV - NUV$  colour. Therefore, just like Fig. 6, even the position of a UV-detected galaxy in the UV colour-colour space can be robustly used to distinguish star-

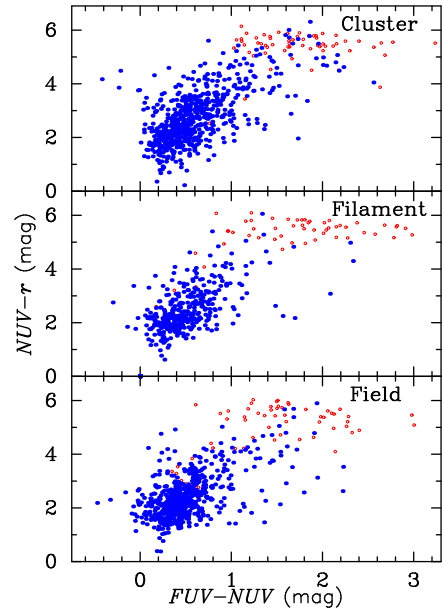


**Figure 8.** The  $NUV - r$  versus  $FUV - NUV$  colour-colour distribution of star-forming and passively-evolving galaxies in three different environments in the Coma supercluster.

forming galaxies from those which are evolving passively (e.g. Gil de Paz et al. 2007).

In a nutshell, in agreement with other studies of the Coma supercluster (Gavazzi et al. 2010; Mahajan, Haines, & Raychaudhury 2010) this section shows that not just the hostile environment of clusters, but all components of the cosmic-web influence the broadband colours of the dwarf and giant galaxies in the Coma supercluster.

## 5 PROPERTIES OF GALAXIES AS A FUNCTION OF DISTANCE FROM CLUSTERS AND SPINE OF FILAMENTS

The observed trend of declining SFR with decreasing cluster-centric distance has been well explored with different datasets in the literature (e.g. Lewis et al. 2002; Gómez et al. 2003; Balogh et al. 2004). Here we reconfirm this trend in the Coma supercluster by analysing the optical and UV properties of galaxies as a function of their distance from the centre of the nearest cluster or group. We extend this analysis a step further by also investigating the impact of the cosmic-web on the properties of galaxies as a function of their distance from the spine of the filaments. In Fig. 9 we show the median  $EW(H\alpha)$ ,  $FUV - NUV$  and the  $g - r$  colour of all as well as non-AGN galaxies as a function of the distance from the nearest group or cluster (Sec. 3.2). It is notable that excluding AGN from the sample only changes the normalization of the radial distribution of galaxies, not the observed trends. Therefore, in the following we discuss the complete sample of galaxies including AGN.

It is evident that the density of environment has an impact on the colours as well as the  $EW(H\alpha)$  of galaxies, such that the median  $FUV - NUV$ , as well as the  $g - r$  colour of galaxies progressively become bluer, and their emission in  $H\alpha$  increases away from the cluster centre. Beyond  $\sim 1.5$  Mpc from the cluster centre, both colours and  $EW(H\alpha)$  seem



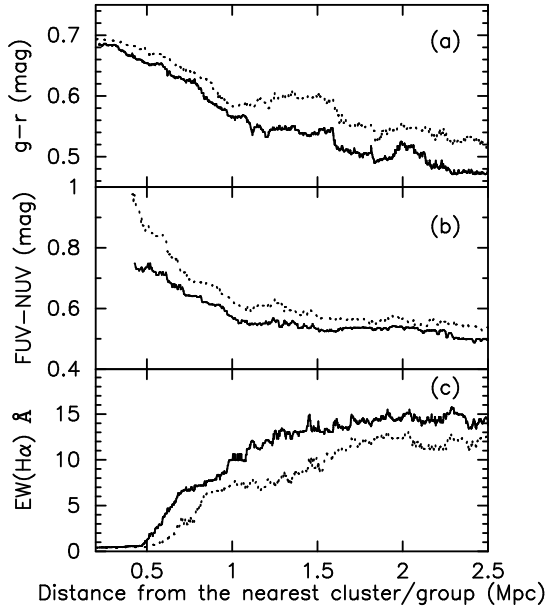


**Figure 9.** The (a)  $g-r$  colour, (b)  $FUV-NUV$  colour and, (c) median  $EW(H\alpha)$  of all (dotted line) and non-AGN (solid line) galaxies as a function of their distance from the nearest cluster or group. These trends show the expected trend that galaxies progressively become bluer and star-forming further away from the centre of clusters.

to approach a constant value close to the respective medians for the void galaxies. Therefore, in agreement with the literature (Gavazzi et al. 2010; Boselli et al. 2014) Fig. 9 shows that the fraction of star-forming, blue galaxies in the Coma supercluster increases with the cluster-centric distance.

In Fig. 10 we show the median  $EW(H\alpha)$ ,  $FUV-NUV$  and the  $g-r$  colour of all as well as non-AGN galaxies in the Coma supercluster as a function of their distance from the spine of the filament (Sec. 3). While both the colours are constant for galaxies within 1 Mpc of the spine, they decline by  $\gtrsim 0.7$  mag beyond it. The trend seen for colours is replicated for the  $EW(H\alpha)$  distribution, which is  $\sim 13\text{\AA}$  within 1 Mpc of the spine, but increases by another  $\sim 3\text{\AA}$  beyond 1 Mpc from it. We tested the statistical significance of these trends by dividing the distributions for all the quantities,  $g-r$ ,  $FUV-NUV$  and  $EW(H\alpha)$  into three radial bins:  $\leq r_{200}^4$ ,  $1-2r_{200}$  and  $> 2r_{200}$ , respectively. The Kolmogorov-Smirnov (K-S) statistic confirms that the probability for the  $EW(H\alpha)$  distributions in the first and third radial bin to have been drawn from the same parent sample is  $2.68e-05$ , while the same for the  $g-r$  and  $FUV-NUV$  colour is  $9.76e-08$  and  $5.73e-14$ , respectively. The same for non-AGN galaxies is  $3.34e-04$ ,  $1.61e-07$  and  $3.07e-10$ , respectively.

Based on these results we choose to limit the radius of filaments in this work to 1 Mpc as mentioned in Sec. 3.3. This is also in agreement with other studies of large-scale filaments based on the SDSS data (Kuutma, Tamm, & Tempel 2017). A caveat in this analysis however is that the SDSS spectra taken with a  $3''$  diameter fibre only represents the

<sup>4</sup>  $r_{200}$  is defined as the radius of the sphere centred at the cluster centre within which the matter density is 200 times the critical density of the Universe.

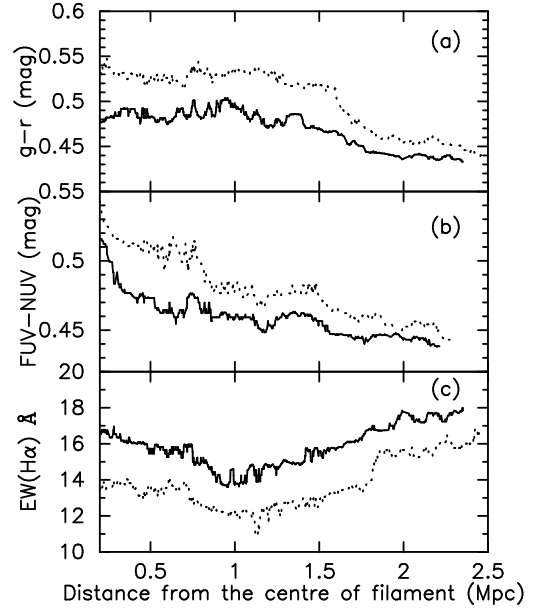


**Figure 10.** The (a)  $g-r$  colour, (b)  $FUV-NUV$  colour and, (c) median  $EW(H\alpha)$  of all (dotted line) and non-AGN (solid line) galaxies in the Coma supercluster as a function of their distance from the spine of the filament. These trends evidently show that some quenching mechanism comes to play as galaxies close in from voids to the spine of filaments.

central bulge of large galaxies. Hence it underestimates the effects of quenching due to various environmental mechanisms primarily occurring in the outer regions of large galaxies (Koopmann, Haynes, & Catinella 2006; Gavazzi et al. 2013).

Together, Figs. 9 and 10 show that galaxies are not just transformed when they assimilate into dense clusters and groups, but also as they approach the seemingly less hostile environment of the filaments. We discuss the implications of this result in the context of the existing literature in the following section.

## 6 DISCUSSION

### 6.1 The significance of large-scale environment for galaxy evolution

In agreement with the literature our results show that the large-scale filaments are critical to transformations in a galaxy prior to its assimilation into clusters or groups. With WHIM temperatures of 3–8 keV and hot gas fraction of  $\sim 10\%$  (e.g. Dietrich et al. 2012), filaments are not just passages leading galaxies to their final destination, but offer a unique environment in which the star formation properties of galaxies can change dramatically over a short period of time (Boué et al. 2008; Fadda et al. 2008; Porter et al. 2008; Mahajan, Raychaudhury, & Pimbblet 2012).

Using a sample of straight filaments selected from the Two-degree field galaxy redshift survey, Porter et al. (2008) showed that the statistical parameter  $\eta$  derived from spectra and acting as a proxy for the SFR, is enhanced between 2–3 Mpc from the edge of the filaments. Moreover, using a sample of Abell clusters ( $z \leq 0.12$ ) selected from the SDSS,

Mahajan, Raychaudhury, & Pimbblet (2012) found that the SFR of galaxies is enhanced on the outskirts of clusters, especially the ones which are fed by more filaments. Elsewhere, such an enhancement in star formation is detected in galaxies on filaments feeding clusters using infrared data (Fadda et al. 2008). These results are intriguing given that most of the star formation in supercluster galaxies at low redshift is contributed by normal galaxies on the periphery of clusters (Haines et al. 2011).

At high redshift ( $z > 0.2$ ), several authors have made use of multi-wavelength data to investigate large-scale filaments. For instance, Geach et al. (2011) combined the *NUV* data from the *GALEX* with the 24- $\mu\text{m}$  data from the *Spitzer* space telescope to investigate a panoramic 15-Mpc region around the supercluster Cl 0016+16 ( $z = 0.55$ ). In agreement with studies at  $z \lesssim 0.1$ , their results (also see Coppin et al. 2012; Darvish et al. 2014, 2015) suggest that the star formation rate of galaxies may increase before they fall into clusters. It has also been suggested that the infalling galaxies may experience a phase of obscured star formation before being effected by the cluster environment (Gallazzi et al. 2009).

Owing to their highly coherent motion along linear filaments (González & Padilla 2009), infalling galaxies are more likely to interact with each other gravitationally relative to their counterparts in voids. Such fly-by interactions can trigger burst of star formation in galaxies falling along filaments (Porter et al. 2008; Mahajan, Raychaudhury, & Pimbblet 2012). But such an enhancement in SFR of galaxies will also increase their star formation efficiency, hence assuming no new infall of gas, such galaxies can become redder relative to similar void galaxies even before encountering the cluster environment. The observations presented in this work as well as other studies (Alpaslan et al. 2016; Kuutma, Tamm, & Tempel 2017; Kraljic et al. 2018) support this hypothesis.

Along with the trend in galaxy properties as a function of cluster-centric distance, now there is also a growing consensus that the properties of galaxies on filaments change as a function of their distance from the backbone of the cosmic web. Using data from the SDSS, Kuutma, Tamm, & Tempel (2017) found a higher elliptical-to-spiral ratio, increasing  $g-i$  colour and decreasing SFR for galaxies moving from voids to filaments. In fact they found the latter trends in the  $g-i$  colour and SFR to be persistent even after separating spiral and elliptical galaxies ( $M_r \leq -20$  mag). Using UV-derived SFR for a sample of  $\sim 12,000$  galaxies ( $z < 0.09$ ) from the Galaxy and Mass Assembly (GAMA) survey, complete to a stellar mass of  $\sim 10^9 M_\odot$ , Alpaslan et al. (2016) showed that the galaxies at the core of filaments are more massive and have lower specific SFR (sSFR;  $\text{SFR}/M^*$ ) relative to their counterparts at the edges of voids. By using a complementary dataset from the GAMA survey, Kraljic et al. (2018) also reached similar conclusions. These results are in agreement with the comparative analysis of properties of galaxies falling into groups isotropically and along filaments. In this comparison, Martínez, Muriel, & Coenda (2016) found that the luminosity function of galaxies in filaments is indistinguishable from the galaxies infalling isotropically, yet their sSFR is lower than the latter, suggesting that galaxies in filaments are more strongly quenched.

Recently Kleiner et al. (2017) examined the HI-to- $M^*$

(HI fraction) of galaxies in the nearby ( $< 181$  Mpc) Universe using data from the 6-degree Field Galaxy Survey and stacking HI data from the HI Parkes all sky survey. They found that while the HI fraction for galaxies with  $M^* < 10^{11} M_\odot$  is the same on filaments and in the control sample, vice versa is true for galaxies more massive than  $10^{11} M_\odot$ . Kleiner et al. (2017) suggested that this result is evidence of cold mode accretion of gas in massive galaxies on filaments, owing to their larger potential well. Our results are in broad agreement with Kleiner et al. (2017) such that in this work we have shown that the intermediate density environment prevalent in the filaments effect dwarfs as well as the giants, although this effect is observed to be more pronounced in the latter. But since we do not find enough galaxies observed in HI for the entire Coma supercluster, in this work we can neither support nor reject the hypothesis of cold mode accretion proposed by Kleiner et al. (2017).

The results presented here are also in broad agreement with those of Gavazzi et al. (2013). Using samples of HI-rich and HI-poor late-type galaxies (LTGs;  $M_{\text{HI}}/M_\odot \geq 9$ ) in the Local supercluster and part of the Coma supercluster from the ALFALFA survey, they showed that HI-rich LTGs represent  $\sim 60\%$  of all LTGs in the low and intermediate density environments, and drop to zero at the centre of the Coma cluster. On the other hand, the frequency of HI-poor LTGs increases with increasing galaxy density.

## 6.2 How does filaments effect galaxies

The census of observed baryons in the local Universe falls short of their estimated contribution of 5 per cent to the total energy budget by a factor of two. Cosmological simulations indicate that rather than condensing into virialized haloes, the missing baryons reside in the filamentary cosmic web. The symbiotic relation between the WHIM ( $10^5 - 10^7$  K), and the constituent galaxies of the filaments is well represented by the discovery of a bent double lobe radio source (DLRS) in a filament feeding the rich cluster Abell 1763 (Edwards et al. 2010a). Assuming that the bend in the jet of the DLRS is due to the ram-pressure experienced by it 3.4 Mpc away from the centre of the cluster, Edwards et al. (2010a) constrained the density of WHIM to be a few times  $10^{-29} \text{ gm cm}^{-3}$ , in agreement with the literature, thereby evidently showing that environmental processes such as ram-pressure stripping may operate much farther away from high density environment of clusters.

By studying the spectroscopic properties of 28 star-forming galaxies ( $z \sim 0.53$ ) in the COSMOS field, Darvish et al. (2015) found that within uncertainties, the EW, EW versus sSFR relation, EW versus  $M^*$  relation, line-of-sight velocity dispersion, dynamical mass, and stellar-to-dynamical mass ratio are similar for filament and field star-forming galaxies. Yet on average, star-forming galaxies on filaments are more metal enriched (0.1–0.5 dex) relative to their field counterparts. Darvish et al. (2015) suggest that the high metallicity may have been caused by the inflow of the enriched intrafilamentary gas into galaxies residing on filaments. However, these high redshift observations are in conflict with the results of Hughes et al. (2013) who found that even though gas-poor galaxies in the Virgo cluster ( $z \sim 0$ ) are typically more metal-rich, statistically the  $M^*$ -metallicity relation is independent of environment. Hughes et al. (2013)

also demonstrated that removal of gas from the outer regions of disc galaxies may increase the observed metallicity by  $\sim 0.1$  dex.

Darvish et al. (2015) also showed that electron densities are significantly lower by a factor of  $\sim 17$  in filament star-forming galaxies compared to those in the field, possibly because of a longer star-formation timescale for filament star-forming galaxies. This, and other aforementioned studies complement the results found in this work and highlight that galaxy properties are not just shaped by  $M^*$  and the large-scale galaxy density, but also the tidal effects of the anisotropic cosmic-web resulting from the interactions between the intra-filamentary gas and galaxies.

### 6.3 Epilogue

Several innovative techniques such as gravitational lensing (Van Waerbeke, Hinshaw, & Murray 2014), stacking of optical photometric data (Zhang et al. 2013), and stacking of x-ray data (Fraser-McKelvie, Pimblet, & Lazendic 2011) are now being employed to discover and characterise various aspects of the cosmic-web. Therefore, observations such as those presented here are crucial not just for strengthening our models of the formations and evolution of the Universe, but also to serve as a benchmark to compare with discoveries and trends observed at higher redshift. In the near future, state-of-the-art technology and global observational projects will play a key role in enhancing our understanding of the cosmic-web. To prepare ahead for these data, while some studies are utilizing simulations to examine the evolution of the cosmic-web properties with redshift (Gheller et al. 2016), others are trying to predict the 21-cm signal of WHIM which may be detected by the Square Kilometer Array (SKA) (Horii et al. 2017, also see Tejos et al. (2016)). Elsewhere, x-ray observations of large-scale filaments have been reported (Werner et al. 2008; Eckert et al. 2015). With an ever expanding database of the known large-scale structures at different epochs, we can hope to understand the evolution of the environment and properties of galaxies in filaments in the near future.

## 7 SUMMARY

We have utilized the optical data from the SDSS DR 12 and UV data from the *GALEX* survey to present a catalogue of UV detected galaxies in the Coma supercluster. We have used DISPERSE to characterize the large-scale filaments, and HDBSCAN algorithm to identify the groups and clusters of galaxies in the Coma supercluster. The key results reported in this work are:

- The position of a galaxy in the  $NUV - r$  versus  $r$  colour-magnitude space and in the  $FUV - NUV$  versus  $NUV - r$  colour-colour space can be robustly used to separate passively-evolving galaxies from their star-forming counterparts in all environments: clusters, filaments and voids.
- Dwarf galaxies are almost always blue except in the dense interiors of the clusters and groups. On the other hand, most of the giants are red in all environments in the Coma supercluster, but their fraction decreases with the environmental density. These trends are seen for the  $FUV - NUV$ , as well as the  $NUV - r$  colour.

- The  $g - r$  and  $FUV - NUV$  colour and  $EW(H\alpha)$  for galaxies vary as a function of their distance from the nearest cluster or group viz., galaxies become redder and emission in  $H\alpha$  declines with their distance from the nearest maximum in density.
- Within a radius of 1 Mpc from the spine of the filament, galaxies become redder and the median  $EW(H\alpha)$  declines closer to the spine of the filament. This transformation in  $g - r$ ,  $FUV - NUV$ , and  $H\alpha$  emission of galaxies is statistically significant, and therefore evidently depicts the key role played by the large-scale filaments in shaping properties of galaxies.

## ACKNOWLEDGEMENTS

We are grateful to Prof. Jasjeet Singh Bagla for his suggestions and comments on several aspects of this work. We acknowledge the high power computing (HPC) facility at IISER Mohali. We are grateful to the anonymous reviewer whose suggestions helped to elucidate this manuscript. Funding for SDSS-III has been provided by the Alfred P. Sloan Foundation, the Participating Institutions, the National Science Foundation, and the U.S. Department of Energy Office of Science. The SDSS-III web site is <http://www.sdss3.org/>. SDSS-III is managed by the Astrophysical Research Consortium for the Participating Institutions of the SDSS-III Collaboration including the University of Arizona, the Brazilian Participation Group, Brookhaven National Laboratory, Carnegie Mellon University, University of Florida, the French Participation Group, the German Participation Group, Harvard University, the Instituto de Astrofisica de Canarias, the Michigan State/Notre Dame/JINA Participation Group, Johns Hopkins University, Lawrence Berkeley National Laboratory, Max Planck Institute for Astrophysics, Max Planck Institute for Extraterrestrial Physics, New Mexico State University, New York University, Ohio State University, Pennsylvania State University, University of Portsmouth, Princeton University, the Spanish Participation Group, University of Tokyo, University of Utah, Vanderbilt University, University of Virginia, University of Washington, and Yale University. This research made use of TOPCAT (Taylor 2005) and the “K-corrections calculator” service available at <http://kcor.sai.msu.ru/>.

Mahajan is funded by the INSPIRE Faculty award (DST/INSPIRE/04/2015/002311), Department of Science and Technology (DST), Government of India. Shobhana was supported by the INSPIRE scholarship for higher education for her BS-MS dual degree at IISERM.

## REFERENCES

- Akamatsu H., et al., 2017, *A&A*, 606, A1  
 Alam S., et al., 2015, *ApJS*, 219, 12  
 Alpaslan M., et al., 2016, *MNRAS*, 457, 2287  
 Baldwin J. A., Phillips M. M., Terlevich R., 1981, *PASP*, 93, 5  
 Balogh M., et al., 2004, *MNRAS*, 348, 1355  
 Bernstein G. M., Nichol R. C., Tyson J. A., Ulmer M. P., Wittman D., 1995, *AJ*, 110, 1507  
 Bianchi L., Herald J., Efremova B., Girardi L., Zobot A., Marigo P., Conti A., Shiao B., 2011, *Ap&SS*, 335, 161

- Bianchi L., Conti A., Shiao B., 2014, *AdSpR*, 53, 900
- Biviano A., Fadda D., Durret F., Edwards L. O. V., Marleau F., 2011, *A&A*, 532, A77
- Bonjean V., Aghanim N., Salomé P., Douspis M., Beelen A., 2018, *A&A*, 609, A49
- Boselli A., et al., 2005, *ApJ*, 629, L29
- Boselli A., et al., 2014, *A&A*, 570, A69
- Boué G., Durret F., Adami C., Mamon G. A., Ilbert O., Cayatte V., 2008, *A&A*, 489, 11
- Budavári T., et al., 2009, *ApJ*, 694, 1281
- Burstein D., Bertola F., Buson L. M., Faber S. M., Lauer T. R., 1988, *ApJ*, 328, 440
- Campello, R. J. G. B., Moulavi, D., Zimek, A., Sander, J., 2013, *Data mining and knowledge discovery*, Vol. 27, Issue 3, 2013, p 344
- Campello, R. J. G. B., Moulavi, D., Zimek, A., Sander, J., 2015, *ACM Trans. Knowl. Discov. Data*, 10, 51
- Cardelli J. A., Clayton G. C., Mathis J. S., 1989, *ApJ*, 345, 245
- Cautun M. C., van de Weygaert R., 2011, *ascl.soft*, ascl:1105.003
- Chilingarian I. V., Zolotukhin I. Y., 2012, *MNRAS*, 419, 1727
- Chincarini G., Rood H. J., 1976, *ApJ*, 206, 30
- Coppin K. E. K., et al., 2011, *MNRAS*, 416, 680
- Coppin K. E. K., et al., 2012, *ApJ*, 749, L43
- Cornett R. H., et al., 1998, *AJ*, 116, 44
- Cortese L., et al., 2005, *ApJ*, 623, L17
- Cortese L., et al., 2007, *MNRAS*, 376, 157
- Cybulski R., Yun M. S., Fazio G. G., Gutermuth R. A., 2014, *MNRAS*, 439, 3564
- Darvish B., Sobral D., Mobasher B., Scoville N. Z., Best P., Sales L. V., Smail I., 2014, *ApJ*, 796, 51
- Darvish B., Mobasher B., Sobral D., Hemmati S., Nayyeri H., Shivaee I., 2015, *ApJ*, 814, 84
- Dietrich J. P., Werner N., Clowe D., Finoguenov A., Kitching T., Miller L., Simionescu A., 2012, *Natur*, 487, 202
- Donas J., Milliard B., Laget M., Buat V., 1990, *A&A*, 235, 60
- Donas J., Milliard B., Laget M., 1995, *A&A*, 303, 661
- Dressler A., 1980, *ApJ*, 236, 351
- Eckert D., et al., 2015, *Natur*, 528, 105
- Edwards L. O. V., Fadda D., Frayer D. T., Lima Neto G. B., Durret F., 2010, *AJ*, 140, 1891
- Edwards L. O. V., Fadda D., Frayer D. T., 2010, *ApJ*, 724, L143
- Ester M., Kriegel H.-P., Sander J., Xu X., 1996, AAAI press, 226
- Fadda D., Biviano A., Marleau F. R., Storrie-Lombardi L. J., Durret F., 2008, *ApJ*, 672, L9
- Fontanelli P., 1984, *A&A*, 138, 85
- Fraser-McKelvie A., Pimbblet K. A., Lazendic J. S., 2011, *MNRAS*, 415, 1961
- Gallazzi A., et al., 2009, *ApJ*, 690, 1883
- Gavazzi G., Fumagalli M., Cucciati O., Boselli A., 2010, *A&A*, 517, A73
- Gavazzi G., et al., 2013, *A&A*, 553, A90
- Geach J. E., Ellis R. S., Smail I., Rawle T. D., Moran S. M., 2011, *MNRAS*, 413, 177
- Génova-Santos R., Atrio-Barandela F., Kitaura F.-S., Mückert J. P., 2015, *ApJ*, 806, 113
- Gheller C., Vazza F., Brügggen M., Alpaslan M., Holwerda B. W., Hopkins A. M., Liske J., 2016, *MNRAS*, 462, 448
- Gil de Paz A., et al., 2007, *ApJS*, 173, 185
- Gómez P. L., et al., 2003, *ApJ*, 584, 210
- González R. E., Padilla N. D., 2009, *MNRAS*, 397, 1498
- Gregory S. A., Thompson L. A., 1978, *ApJ*, 222, 784
- Haines C. P., Gargiulo A., La Barbera F., Mercurio A., Merluzzi P., Busarello G., 2007, *MNRAS*, 381, 7
- Haines C. P., Gargiulo A., Merluzzi P., 2008, *MNRAS*, 385, 1201
- Haines C. P., Busarello G., Merluzzi P., Smith R. J., Raychaudhury S., Mercurio A., Smith G. P., 2011, *MNRAS*, 412, 145
- Hammer D., Hornschemeier A. E., Mobasher B., Miller N., Smith R., Arnouts S., Milliard B., Jenkins L., 2010, *ApJS*, 190, 43
- Hammer D. M., Hornschemeier A. E., Salim S., Smith R., Jenkins L., Mobasher B., Miller N., Ferguson H., 2012, *ApJ*, 745, 177
- Hicks A. K., Mushotzky R., 2005, *ApJ*, 635, L9
- Hogg, D. W., Blanton, M. R., Brinchmann, J., et al. 2004, *ApJ*, 601, L29
- Horii T., Asaba S., Hasegawa K., Tashiro H., 2017, *PASJ*, 69, 73
- Hughes T. M., Cortese L., Boselli A., Gavazzi G., Davies J. I., 2013, *A&A*, 550, A115
- Jauzac M., et al., 2012, *MNRAS*, 426, 3369
- Kauffmann G., et al., 2003, *MNRAS*, 341, 54
- Kennicutt R. C., Jr., 1998, *ARA&A*, 36, 189
- Kewley L. J., Dopita M. A., Sutherland R. S., Heisler C. A., Trevena J., 2001, *ApJ*, 556, 121
- Kim K.-T., Kronberg P. P., Giovannini G., Venturi T., 1989, *Natur*, 341, 720
- Kim S., et al., 2016, *ApJ*, 833, 207
- Kleiner D., Pimbblet K. A., Jones D. H., Koribalski B. S., Serra P., 2017, *MNRAS*, 466, 4692
- Koopmann R. A., Haynes M. P., Catinella B., 2006, *AJ*, 131, 716
- Kraljic K., et al., 2018, *MNRAS*, 474, 547
- Kuutma T., Tamm A., Tempel E., 2017, *A&A*, 600, L6
- Lewis I., et al., 2002, *MNRAS*, 334, 673
- Mahajan S., Haines C. P., Raychaudhury S., 2010, *MNRAS*, 404, 1745
- Mahajan S., Haines C. P., Raychaudhury S., 2011, *MNRAS*, 412, 1098
- Mahajan S., Raychaudhury S., Pimbblet K. A., 2012, *MNRAS*, 427, 1252
- Mahajan S., 2013, *MNRAS*, 431, L117
- Martin D. C., et al., 2005, *ApJ*, 619, L1
- Martínez H. J., Muriel H., Coenda V., 2016, *MNRAS*, 455, 127
- Mobasher B., et al., 2003, *ApJ*, 587, 605
- McInnes L., Healy J., 2017, *IEEE International Conference on Data Mining Workshops (ICDMW)*, p33
- McInnes L., Healy J., Astels, S., 2017b, *Journal of Open Source Software*, 2(11), 205
- Muldrew S. I., et al., 2012, *MNRAS*, 419, 2670
- O'Connell R. W., 1999, *ARA&A*, 37, 603
- Parekh V., Durret F., Padmanabh P., Pandge M. B., 2017, *MNRAS*, 470, 3742
- Porter S. C., Raychaudhury S., 2007, *MNRAS*, 375, 1409
- Porter S. C., Raychaudhury S., Pimbblet K. A., Drinkwater M. J., 2008, *MNRAS*, 388, 1152
- Rines K., Geller M. J., Kurtz M. J., Diaferio A., 2005, *AJ*, 130, 1482
- Schaap W. E., van de Weygaert R., 2000, *A&A*, 363, L29
- Schawinski K., et al., 2007, *ApJS*, 173, 512
- Schubert E., Sander J., Ester M., Kriegel H.-P., Xu X., 2017, *TODS*, Vol. 42, Issue 3, p 19
- Smith R. J., et al., 2010, *MNRAS*, 408, 1417
- Smith R. J., Lucey J. R., Carter D., 2012, *MNRAS*, 421, 2982
- Smith R. J., Lucey J. R., Price J., Hudson M. J., Phillipps S., 2012, *MNRAS*, 419, 3167
- Sousbie T., 2011, *MNRAS*, 414, 350
- Sousbie T., Pichon C., Kawahara H., 2011, *MNRAS*, 414, 384
- Sun M., Donahue M., Roediger E., Nulsen P. E. J., Voit G. M., Sarazin C., Forman W., Jones C., 2010, *ApJ*, 708, 946
- Tanimura H., Hinshaw G., McCarthy I. G., Van Waerbeke L., Ma Y.-Z., Mead A., Hojjati A., Tröster T., 2017, *arXiv*, arXiv:1709.05024
- Taylor M. B., 2005, *ASPC*, 347, 29
- Tejos N., et al., 2016, *MNRAS*, 455, 2662
- Tran K.-V. H., Saintonge A., Moustakas J., Bai L., Gonzalez A. H., Holden B. P., Zaritsky D., Kautsch S. J., 2009, *ApJ*, 705, 809
- Van Waerbeke L., Hinshaw G., Murray N., 2014, *PhRvD*, 89, 023508
- Verdugo M., Lerchster M., Böhringer H., Hildebrandt H., Ziegler

- B. L., Erben T., Finoguenov A., Chon G., 2012, MNRAS, 421, 1949
- Wang Q. D., Owen F., Ledlow M., 2004, ApJ, 611, 821
- Werner N., Finoguenov A., Kaastra J. S., Simionescu A., Dietrich J. P., Vink J., Böhringer H., 2008, A&A, 482, L29
- Wright E. L., et al., 2010, AJ, 140, 1868-1881
- Wyder T. K., et al., 2007, ApJS, 173, 293
- Zabludoff A. I., Mulchaey J. S., 1998, ApJ, 496, 39
- Zhang Y., Dietrich J. P., McKay T. A., Sheldon E. S., Nguyen A. T. Q., 2013, ApJ, 773, 115

This paper has been typeset from a  $\text{\TeX}/\text{\LaTeX}$  file prepared by the author.